Inverse moments equilibria for helical anisotropic systems

W. A. Cooper

Centre de Recherches en Physique des Plasmas, Association Euratom—Confédération Suisse, École Polytechnique Fédérale de Lausanne, 21, Av. des Bains, CH-1007 Lausanne, Switzerland

S. P. Hirshman

Fusion Energy Division, Oak Ridge National Laboratory, P.O. Box Y, Oak Ridge, Tennessee 37831

M. C. Depassier

Facultad de Física, Universidad Católica de Chile, Casilla 114-D, Santiago, Chile

An energy functional is devised for magnetic confinement schemes that have anisotropic plasma pressure. The minimization of this energy functional is demonstrated to reproduce components of the magnetohydrodynamic (MHD) force balance relation in systems with helical symmetry. An iterative steepest descent procedure is applied to the Fourier moments of the inverse magnetic flux coordinates to minimize the total energy and thus generate anisotropic pressure MHD equilibria. Applications to straight ELMO Snaky Torus (NTIS Document No. DE-84002406) configurations that have a magnetic well on the outermost flux surfaces have been obtained.

I. INTRODUCTION

Helical magnetic axis stellarator configurations with circular coils constitute a potentially very attractive magnetic fusion energy reactor concept because they are steady state devices that have finite rotational transform and can be built modularly. However, they possess a magnetic hill in the vacuum state and are therefore susceptible to large scale magnetohydrodynamic (MHD) instabilities. To construct a device that has a magnetic well, one possible approach is to deform the plasma boundary into a bean shape with a linked toroidal hard core. This configuration is called a Heliac.[1,2] A different scheme that does not sacrifice the volume utilization and the modularity is the ELMO Snaky Torus conceived by Furth and Boozer.[3] This type of device is a helical axis stellarator that has displaced circular coils that generate a toroidal (axial) magnetic field and has an energetic electron population that provides stability in a similar way as the hot electron rings in the ELMO Bumpy Torus concept.[4]

To obtain anisotropic pressure MHD equilibria in the limit of helical symmetry, we formulate a positive definite energy minimization procedure that employs a steepest descent method to determine the Fourier moments of the nonignorable geometric coordinates and of a periodic poloidal angle renormalization parameter in terms of the magnetic flux coordinates.[5] Using this approach, we generate numerically straight ELMO Snaky Torus equilibria.

Previously, Miller has calculated helically symmetric ELMO Snaky Torus equilibria.[6] His work is different from ours in three important aspects. First, he employs a standard direct method to obtain the helical flux as a function of the nonignorable geometric coordinates. We use an inverse moments method that can be straightforwardly extended to three dimensions.[5] Second, Miller advocates transport arguments to prescribe zero averaged plasma current along the magnetic field lines. We define an effective axial plasma current that vanishes on each flux surface from which we recover the zero current condition of the isotropic pressure

model when $p_{\parallel} = p_{\perp}$.[7] Third, he searches for the conditions that will generate a global magnetic well and finds that a hot electron population that occupies almost the entire volume of the plasma is required. We rely on a more local hot electron layer to obtain a magnetic well on the outermost flux surfaces only and then tailor the thermal pressure profiles to have weak radial gradients in regions where a magnetic hill prevails. Consequently, the work we present here is complementary to that of Ref. 6.

In Sec. II, we discuss the magnetic field geometry. In Sec. III, we discuss the MHD force balance, define an effective axial current, and present the corresponding rotational transform. In Sec. IV, we construct an energy functional and demonstrate that its minimization with respect to an artificial time parameter yields components of the MHD force balance relation in helical symmetry. The Fourier moments steepest descent procedure is outlined. In Sec. V, we derive the radial force balance. In Sec. VI, we present applications to a straight ELMO Snaky Torus configuration, and, in Sec. VII, we discuss the summary and conclusions.

II. MAGNETIC FIELD GEOMETRY

The Maxwell equation $\nabla \cdot \mathbf{B} = 0$, in a magnetic confinement system with a coordinate of symmetry ϕ, implies that the magnetic field in contravariant representation has the form

$$\mathbf{B} = \nabla\phi \times \nabla\Psi + \sqrt{g}B^{\phi}\nabla\rho \times \nabla\theta$$
$$= \nabla\phi \times \nabla\Psi + \nabla\Phi \times \nabla\theta_{*}, \tag{1}$$

where $2\pi\Psi$ and $2\pi\Phi$ are the helical and axial magnetic fluxes, respectively, which are functions only of the radial variable ρ. The variable θ_* corresponds to a poloidal angle in a flux coordinate system in which the magnetic field lines are straight. It can be expressed in terms of any arbitrary poloidal angle θ by the relation $\theta_* = \theta + \lambda(\rho,\theta)$, where λ is a periodic renormalization parameter.[5] In systems with helical symmetry, it is convenient to identify the ignorable angu-
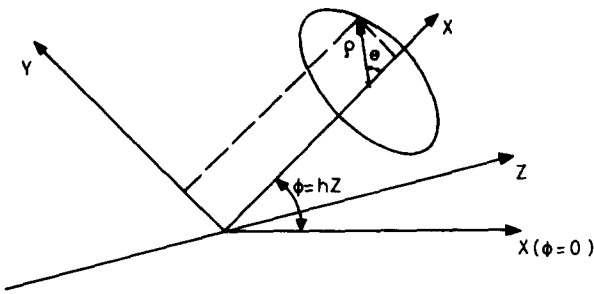
FIG. 1. Schematic diagram of the geometry in a system with helical symmetry. The coordinate system (X,Y,ϕ) constitutes a rotating Cartesian frame about the Z axis. These coordinates are related to the static Cartesian coordinates (X_0,Y_0,Z) through $X = X_0 \cos\phi + Y_0 \sin\phi$, $Y = -X_0 \sin\phi + Y_0 \cos\phi$, and $\phi = hZ$. Note that $X_0 = X(\phi = 0)$ and $Y_0 = Y(\phi = 0)$. The elliptical contour identifies a flux surface with label ρ of a magnetic flux coordinate system (ρ,θ,ϕ).

lar coordinate ϕ as $\phi = hZ$, where h is the helical pitch and Z is the axial distance. With this choice for ϕ, the Jacobian of the transformation from the rotating Cartesian frame (X,Y,ϕ) to the magnetic flux coordinates (ρ,θ,ϕ) and the metric elements g_{ij} acquire very simple forms.[8] A schematic diagram of the geometry in systems with helical symmetry is shown in Fig. 1.

The magnetic field components in the covariant representation are $B_\theta = g_{\theta\theta}B^\theta + g_{\theta\phi}B^\phi$, $B_\phi = g_{\theta\phi}B^\theta + g_{\phi\phi}B^\phi$, and $B_\rho = g_{\rho\theta}B^\theta + g_{\rho\phi}B^\phi$. The magnetic field components in the contravariant representation are $B^\phi = (1 + \partial\lambda/\partial\theta)\Phi'/\sqrt{g}$ and $B^\theta = \iota\Phi'/\sqrt{g}$,[5] where $\iota(\rho) \equiv \Psi'/\Phi'$ is the rotational transform and the primes denote derivatives of flux surface quantities with respect to ρ.

III. EFFECTIVE PLASMA CURRENT

In systems with a coordinate of symmetry, the vanishing of the MHD force balance component along the magnetic field lines is invoked to demonstrate that the perpendicular pressure $p_\perp$ is related to the parallel pressure $p_\parallel$, that both are functionals of ρ and B, and that the MHD force reduces to

$$\mathbf{F} = -\frac{\partial p_\parallel}{\partial \rho}\nabla\rho + \mathbf{K}\times\mathbf{B}, \qquad (2)$$

where $\mathbf{K} \equiv \nabla\times(\sigma\mathbf{B})$ is the effective current density and $\sigma = 1/\mu_0 - (\partial p_\parallel/\partial B)/B$ is the anisotropy parameter.[9]

In an equilibrium state, we have that $\mathbf{F} = 0$. Consequently, $\mathbf{K}$ satisfies the same properties as the current density $\mathbf{J}$ in the isotropic pressure limit, namely that $\mathbf{K}\cdot\nabla\rho = 0$ and $\nabla\cdot\mathbf{K} = 0$. Therefore, in analogy with the scalar pressure case, we define an effective axial current

$$I(\rho) = \int\int d\rho\, d\theta\, \sqrt{g}(\mathbf{K}\cdot\nabla\phi) = \int d\theta(\sigma B_\theta). \qquad (3)$$

Expanding B_θ as shown in the previous section, we can derive an expression for $\iota(\rho)$ that corresponds to a prescribed $I(\rho)$,

$$\iota(\rho) = \frac{I(\rho) - \int d\theta(\sigma\Phi'/\sqrt{g})(1 + \partial\lambda/\partial\theta)g_{\theta\phi}}{\int d\theta(\sigma\Phi'/\sqrt{g})g_{\theta\theta}}. \qquad (4)$$

For configurations of the stellarator type, the absence of induced currents makes $I(\rho) = 0$ within each flux surface a natural choice.

IV. ENERGY MINIMIZATION

We define the total energy of the system as

$$W = \int\int\int d^3x\left(\frac{B^2}{2\mu_0} + \frac{p_\parallel(\rho,B)}{(\Gamma - 1)}\right), \qquad (5)$$

where we express the parallel pressure as

$$p_\parallel(\rho,B) = M(\rho)[\Phi'(\rho)]^\Gamma \frac{1 + p(\rho,B)}{\langle 1 + p(\rho,B)\rangle^\Gamma}, \qquad (6)$$

in which $M(\rho)$ represents the mass function introduced previously in the scalar pressure formulation of this problem[5] and is a flux surface quantity, $p(\rho,B)$ is the energetic species contribution to the pressure, and $\langle p(\rho,B)\rangle \equiv \int\int d\theta\, d\phi \times \sqrt{g}p(\rho,B)$ denotes its flux surface average. For an adiabatic index $\Gamma > 1$ (that we typically take to be the ratio of specific heats 5/3), W is positive definite which guarantees that the minimum energy state corresponds to an MHD equilibrium. We then vary the energy W with respect to an artificial time parameter t in such a way that the magnetic fluxes Φ and Ψ, the mass M, and the magnetic coordinates ρ, θ, ϕ remain invariant.[5] This also entails a variation of the function p which is carried out through its dependency on B, namely,

$$\frac{dp}{dt} = \frac{\partial p}{\partial B}\frac{\partial B}{\partial t}. \qquad (7)$$

As a result, we obtain for a fixed boundary calculation that

$$\frac{dW}{dt} = -\int\int\int d\rho\, d\theta\, d\phi\, F_X \frac{\partial X}{\partial t}$$
$$-\int\int\int d\rho\, d\theta\, d\phi\, F_Y \frac{\partial Y}{\partial t}$$
$$-\int\int\int d\rho\, d\theta\, d\phi\, F_\lambda \frac{\partial\lambda}{\partial t}, \qquad (8)$$

where

$$F_X = \frac{\partial}{\partial\theta}\left\{\frac{\sigma\iota(\Phi')^2}{\sqrt{g}}\left[\iota\frac{\partial X}{\partial\theta} - \left(1 + \frac{\partial\lambda}{\partial\theta}\right)Y\right]\right.$$
$$\left. + \frac{1}{h}\frac{\partial Y}{\partial\rho}\left(\frac{B^2}{2\mu_0} + p_\perp\right)\right\}$$
$$- \frac{\partial}{\partial\rho}\left[\frac{1}{h}\frac{\partial Y}{\partial\theta}\left(\frac{B^2}{2\mu_0} + p_\perp\right)\right]$$
$$- \frac{\sigma(\Phi')^2}{\sqrt{g}}\left(1 + \frac{\partial\lambda}{\partial\theta}\right)\left[\iota\frac{\partial Y}{\partial\theta} + \left(1 + \frac{\partial\lambda}{\partial\theta}\right)X\right], \quad (9)$$

and

$$F_Y = \frac{\partial}{\partial\theta}\left\{\frac{\sigma\iota(\Phi')^2}{\sqrt{g}}\left[\iota\frac{\partial Y}{\partial\theta} + \left(1 + \frac{\partial\lambda}{\partial\theta}\right)X\right]\right.$$
$$\left. - \frac{1}{h}\frac{\partial X}{\partial\rho}\left(\frac{B^2}{2\mu_0} + p_\perp\right)\right\}$$

$$+ \frac{\partial}{\partial \rho}\left[\frac{1}{h}\frac{\partial X}{\partial \theta}\left(\frac{B^2}{2\mu_0}+p_\perp\right)\right]$$

$$+ \frac{\sigma(\Phi')^2}{\sqrt{g}}\left(1+\frac{\partial\lambda}{\partial\theta}\right)\left[\iota\frac{\partial X}{\partial\theta}-\left(1+\frac{\partial\lambda}{\partial\theta}\right)Y\right]. \quad (10)$$

An alternative form for the force balance relation given in Eq. (2) is $\mathbf{F} = -\nabla(p_\perp + B^2/2\mu_0) + (\mathbf{B\cdot\nabla})(\sigma\mathbf{B})$. Then, noting from Fig. 1 that $\nabla Y\times\nabla\phi = h(\nabla X - Y\nabla\phi)$ and $\nabla\phi\times\nabla X = h(\nabla Y + X\nabla\phi)$, it is easy to show that $(\mathbf{B\cdot\nabla})(\nabla Y\times\nabla\phi) = hB^\phi(\nabla Y + X\nabla\phi)$ and $(\mathbf{B\cdot\nabla})(\nabla\phi\times\nabla X) = -hB^\phi(\nabla X - Y\nabla\phi)$. With these expressions it becomes a straightforward vector algebra exercise to demonstrate that the force components that result from the variation of the energy are $F_X = \sqrt{g}\nabla Y\times\nabla\phi\cdot\mathbf{F}/h$ and $\mathbf{F}_Y = \sqrt{g}\nabla\phi\times\nabla X\cdot\mathbf{F}/h$. These constitute the covariant components of the MHD force balance relation in the rotating Cartesian frame. The remaining component in Eq. (8),

$$F_\lambda = \frac{\partial}{\partial\theta}[(\sigma B_\phi)\Phi'], \quad (11)$$

corresponds to $-\sqrt{g}\Phi'\mathbf{B}\times\nabla\rho\cdot\mathbf{F}/B^2$, which is basically the binormal component of the force balance. An equilibrium state is achieved when these force components simultaneously vanish. Note that the vanishing of F_λ makes the function (σB_ϕ) a flux surface quantity.

The next step in the procedure to obtain an MHD equilibrium is to expand each term of Eq. (8) in a Fourier series. The path of steepest descent that minimizes the energy of the system corresponds to

$$\frac{\partial X_m}{\partial t} = F_{Xm}(\rho), \quad (12)$$

$$\frac{\partial Y_m}{\partial t} = F_{Ym}(\rho), \quad (13)$$

and

$$\frac{\partial \lambda_m}{\partial t} = F_{\lambda m}(\rho). \quad (14)$$

The subscript m denotes the Fourier amplitude of the expression with respect to the poloidal mode number m. The Fourier moments of X, Y, and λ are thus advanced iteratively in t until all of the force amplitudes vanish within some tolerance. The convergence of these equations is accelerated, however, with a second order Richardson scheme.[5] The numerical procedure was previously developed and applied to axisymmetric and three-dimensional systems with isotropic pressure.[5] In this article, we extend the method to helical devices with anisotropic pressure dynamics.

V. RADIAL FORCE BALANCE

To diagnose an equilibrium obtained with the energy minimization scheme we have described, it is useful to evaluate the radial component of the force balance relation (2),

$$F_\rho = \sqrt{g}\nabla\theta\times\nabla\Phi\cdot\mathbf{F}$$

$$= -\frac{\Phi'}{\sqrt{g}}\left[\frac{\sqrt{g}}{\Phi'}\frac{\partial p_\parallel}{\partial\rho} + \iota\frac{\partial(\sigma B_\theta)}{\partial\rho}\right.$$

$$\left. + \left(1+\frac{\partial\lambda}{\partial\theta}\right)\frac{\partial(\sigma B_\phi)}{\partial\rho} - \iota\frac{\partial(\sigma B_\rho)}{\partial\theta}\right]. \quad (15)$$

This expression set to 0 corresponds to the MHD equilibrium equation (the anisotropic helical Grad–Schlüter–Shafranov equation) in the magnetic flux coordinates that was solved by Miller to obtain straight ELMO Snaky Torus equilibria.[6]

VI. APPLICATION

We have implemented a computer code to obtain helically symmetric MHD equilibria that have anisotropic plasma pressure with the steepest descent energy minimization procedure we have described. This is a variant of the isotropic pressure code HESMEC.[10]

An appropriate model for electron cyclotron resonance heated (ECRH) energetic electron species is a Maxwellian distribution function with a scale factor that loads particles in the perpendicular velocity direction,

$$F_h(E,\mu,\rho) = N_h(\rho)\left(\frac{M_e}{2\pi T_h(\rho)}\right)^{3/2}$$

$$\times\exp\left(-\frac{E}{T_h(\rho)}\right)\left(\frac{\mu B_M(\rho)}{E}\right)^L, \quad (16)$$

where N_h is an average hot electron density on a flux surface, T_h is the electron temperature, M_e is the electron mass, B_M is the minimum value of the magnetic field B on a flux surface, E is the energy, μ is the magnetic moment, and the integer L is the anisotropy factor. Typical distribution functions in $v_\perp$-$v_\parallel$ space for different values of L are shown in Fig. 2. A hot electron pressure moment $p(\rho,B)$ that is consistent with this type of distribution function is

$$p(\rho,B) = p_h(\rho)[B_M(\rho)/B]^L. \quad (17)$$

We choose to represent the function $p_h(\rho)$ by a Gaussian centered about a flux surface $\rho = \rho_a$ with a width Δ,

$$p_h(\rho) = p_0\exp[-(\rho-\rho_a)^2/2\Delta^2]. \quad (18)$$

To describe the mass profile, we choose

$$M(\rho) = M_0\{M_r + (1-M_r)[1-(\rho/\rho_a)^l]\}[1+p_h(\rho)]^\Gamma \quad (19a)$$

for $\rho < \rho_a$ and

$$M(\rho) = M_0 M_r[1-(\rho-\rho_a)/(1-\rho_a)]^2[1+p_h(\rho)]^\Gamma \quad (19b)$$

for $\rho\geqslant\rho_a$, where M_0 is an arbitrary constant, M_r is a constant between 0 and 1, and

$$l = 2[\rho_a/(1-\rho_a)][M_r/(1-M_r)], \quad (20)$$

so that M is a continuously differentiable function. The philosophy that underlies the choice for the mass profile we have made is the generation of pressure profiles that have very weak or nonexistent radial gradients in regions where there is a magnetic hill in the "vacuum" which would be susceptible to MHD instabilities, and we concentrate all the gradients in the region of magnetic well. In this context, the term "vacuum" means the equilibrium state with zero thermal pressure but finite hot electron pressure.

All the numerical calculations we present have zero effective axial plasma current prescribed within each flux surface, satisfy the mirror stability criterion $\tau\equiv\partial(\sigma B)/\partial B > 0$ everywhere,[9] have $\Phi'\equiv\rho$, and are carried out on a grid with

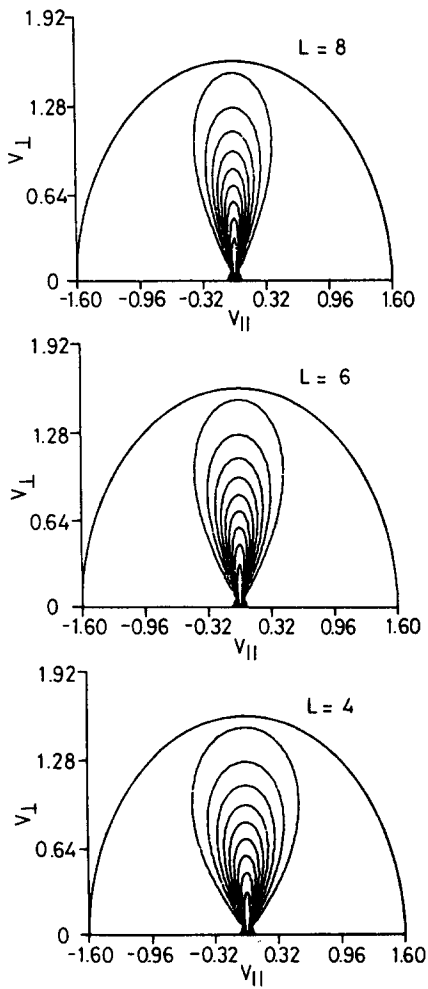FIG. 2. Contours of the constant number of particles in $v_{\parallel}$-$v_{\perp}$ space of a loaded Maxwellian distribution function with $L = 8$ (top figure), $L = 6$ (middle figure), and $L = 4$ (bottom figure).
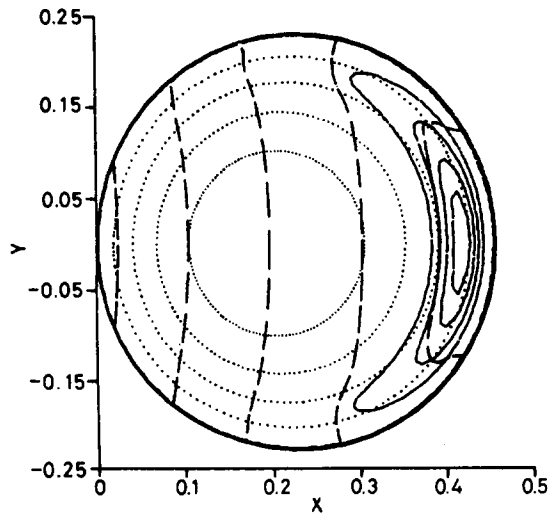

FIG. 3. The axial (Φ) magnetic flux surfaces (the nearly circular contours), the mod-B contours (the nearly vertical lines), and the hot electron pressure surfaces (the moon-shaped contours) defined by $(p_{\parallel} + 2p_{\perp})/3$ of a reference straight ELMO Snaky Torus equilibrium with a minor radius of 0.23 m, $h = 1.0/(0.375 \text{ m})$, $M_0 = 3.4\times10^{-4}$, $M_r = 0.15$, $\rho_a = 0.93$, $p_0 = 9.5$, $\Delta = 0.1$, and $L = 8$.

41 radial points, 25 poloidal points, and 8 poloidal mode numbers.

A. Reference equilibrium

A reference equilibrium case in the "vacuum" is obtained for a configuration that has a circular cross section with a minor radius of 0.23 m, a helical pitch $h = 1.0/(0.375$ m) with $M_0 = 3.4\times10^{-4}$, $M_r = 0.15$, $\rho_a = 0.93$, $p_0 = 9.5$, $\Delta = 0.1$, and $L = 8$. The flux surfaces, the mod-B surfaces, and the energetic electron pressure surfaces for this case are shown in Fig. 3. This equilibrium has a $\beta_{\text{th}} \simeq 0$ and $\beta_h = 0.7\%$, where we have defined

$$\beta_{\text{th}} \equiv \frac{\iiint d^3x\, p_{\text{th}}}{\iiint d^3x\,(B^2/2\mu_0)}, \tag{21}$$

and

$$\beta_h = \frac{\iiint d^3x\,(\tfrac{2}{3}p_{\perp h} + \tfrac{1}{3}p_{\parallel h})}{\iiint d^3x\,(B^2/2\mu_0)}, \tag{22}$$
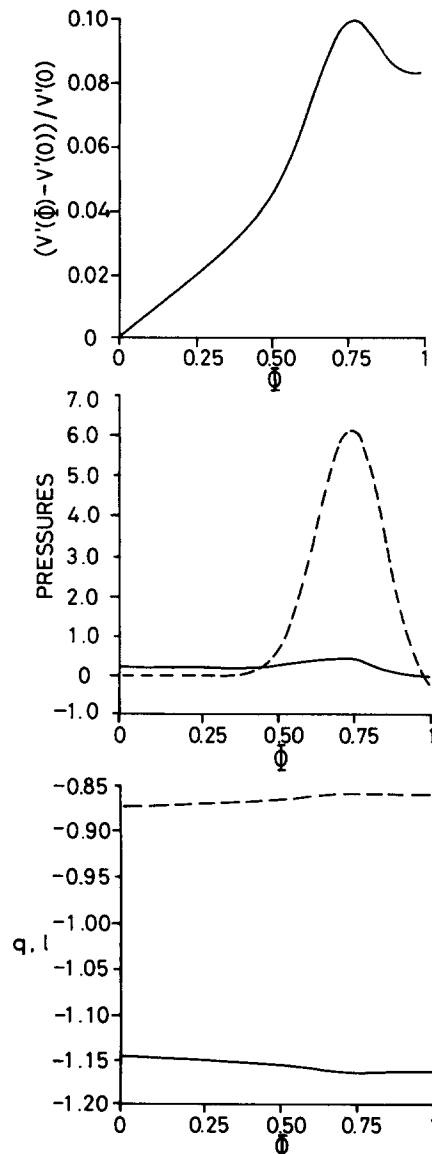

FIG. 4. The differential volume profile (top figure), the hot electron pressure profile $\langle p_{\parallel} + 2p_{\perp}\rangle/3$ (dashed line in middle figure), the thermal pressure profile (solid line in middle figure), the ι profile (dashed line in bottom figure), and q profile (solid line in bottom figure) as functions of the axial flux Φ for the reference equilibrium shown in Fig. 3.

and the subscripts th and h refer to the thermal and hot particle components, respectively. The minimum value of $\mu_0\tau$ is 0.017 and the peak value of β_h is 4.6%. In Fig. 4, we plot the differential volume, pressures, and ι and $q \equiv 1/\iota$ radial profiles. The differential volume profile shows that a magnetic hill exists on the inner flux surfaces. A magnetic well develops, however, on the outer flux surfaces where the hot electron pressure gradient is strongly negative. The ι profile shown corresponds to that in the rotating frame of reference. One must add unity to it to obtain the rotational transform values in the laboratory frame.[7]

B. Variation of hot electron layer radial width

We vary the radial extent of the band of hot electrons by changing the parameter Δ. The flux surfaces, mod-B contours, and hot electron pressure contours for $\Delta = 0.1$ (the
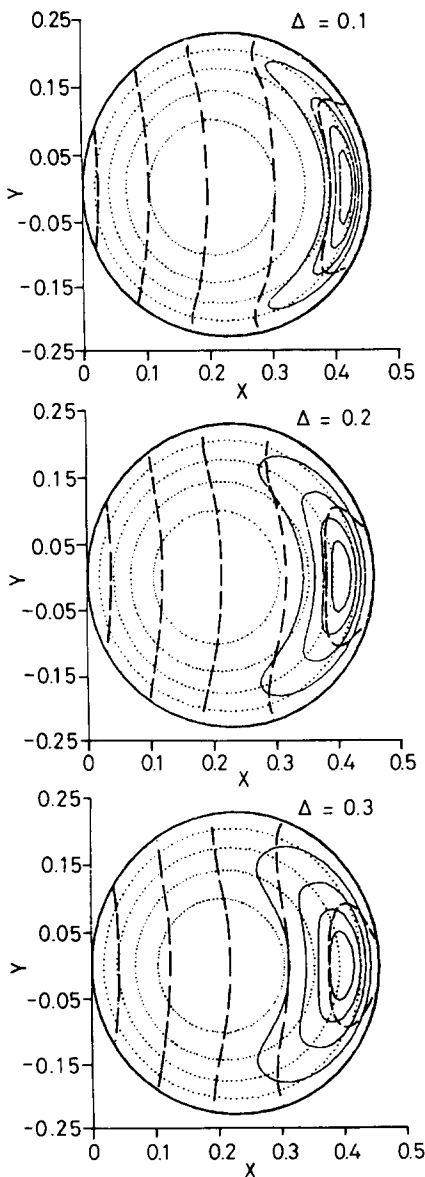
FIG. 5. The axial (Φ) magnetic flux surfaces (the nearly circular contours), the mod-B contours (the nearly vertical lines), and the hot electron pressure surfaces (the moon-shaped contours) for the reference equilibria that have $\Delta = 0.1$ (top figure), $\Delta = 0.2$ (middle figure), and $\Delta = 0.3$ (bottom figure).
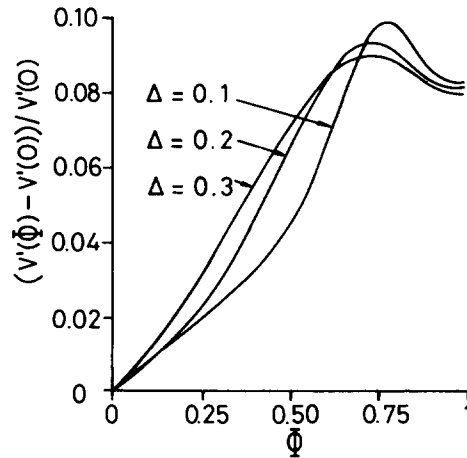
FIG. 6. The differential volume profiles for the reference equilibria that have $\Delta = 0.1$, $\Delta = 0.2$, and $\Delta = 0.3$ as functions of the axial flux Φ.

reference case), $\Delta = 0.2$, and $\Delta = 0.3$ are presented in Fig. 5. As Δ increases, the radial extent of the hot electron layer broadens and also its peak moves slightly toward the magnetic axis. The flux surfaces and mod-B contours are not noticeably altered. The differential volume profiles for each of these cases are shown in Fig. 6. As Δ increases, the magnetic well becomes slightly broader and shallower as the negative radial hot electron pressure gradient becomes less localized, which is evident in Fig. 7. To obtain a hot electron induced local magnetic well that extends to the plasma edge, a $\beta_h = 1.2\%$ with $\Delta = 0.2$ and a $\beta_h = 1.5\%$ with $\Delta = 0.3$ are required, respectively.

C. Variation of hot electron poloidal extent

We vary the poloidal extent of the band of hot electrons by changing the integer L. The flux surfaces, mod-B contours, and hot electron pressure contours for $L = 8$ (the reference case), $L = 6$, and $L = 4$ are presented in Fig. 8. All these equilibria have $\beta_h \simeq 0.7\%$. As L increases, the hot electrons become more localized poloidally about the point at which the magnitude of the magnetic field is a minimum
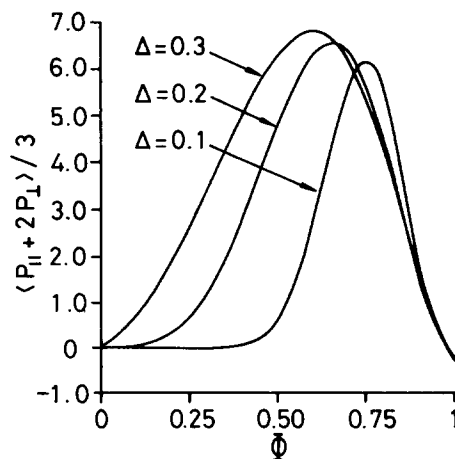
FIG. 7. The hot electron pressure profiles $\langle p_\parallel + 2p_\perp \rangle/3$ for the reference equilibria that have $\Delta = 0.1$, $\Delta = 0.2$, and $\Delta = 0.3$ as functions of the axial magnetic flux Φ.
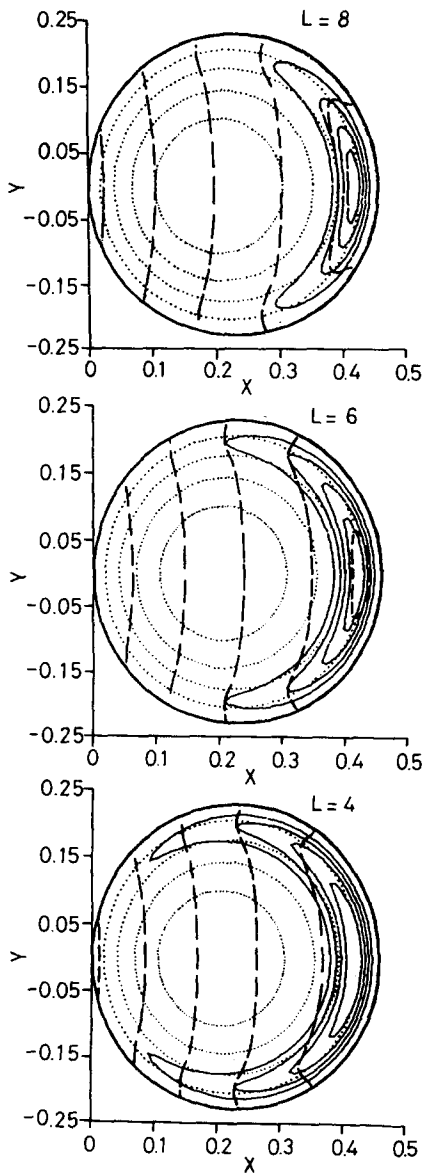
FIG. 8. The axial (Φ) magnetic flux surfaces (the nearly circular contours), the mod-B contours (the nearly vertical lines), and the hot electron pressure surfaces (the moon-shaped contours) for the reference equilibria that have $L = 8$ (top figure), $L = 6$ (middle figure), and $L = 4$ (bottom figure).

on the flux surface where these electrons are radially concentrated. The flux surfaces and the mod-B contours are not noticeably altered, nor are the differential volume profiles. However, of these cases, the $L = 8$ example seems the most realistic because the hot electron pressure contours are more closely aligned with the mod-B contours, which is a result one would expect with energy deposition from an ECRH source. For $L > 8$, the mirror stability criterion is violated for the $\beta_h \simeq 0.7\%$ required to produce a magnetic well in the plasma edge region.

D. Variation of thermal beta

We vary β_{th}, while keeping β_h fixed as well as controlling the thermal pressure gradients in the region of vacuum magnetic hill, by changing M_0, M_r, and p_0. The flux surfaces, the mod-B contours, and the hot electron contours for

$\beta_{th} \simeq 0$ (the reference case), for $\beta_{th} \simeq 2\% (M_0 = 8.0 \times 10^{-3}$, $M_r = 0.3$, $p_0 = 0.64$), and for $\beta_{th} \simeq 18\%$ $(M_0 = 6.9 \times 10^{-2}, M_r = 0.93, p_0 = 0.067)$ are presented in Fig. 9. All these cases have $\beta_{th} \simeq 0.7\%$. The mod-B contours are affected by the change in β_{th} but only on the outermost flux surfaces. The flux surfaces and the hot electron pressure contours are not noticeably altered. The pressure profiles are shown in Fig. 10. As can be seen, we have tailored the thermal pressure profile so that its radial gradients remain close to zero in the regions where there is a magnetic hill in the vacuum state. As a consequence, there is no perceptible shift of the magnetic axis with increasing β_{th}. The differential volume profiles that appear in Fig. 11 show a deepening of the magnetic well induced by the thermal pressure gradient as β_{th} increases, but no significant change of the region and magnitude of the vacuum magnetic hill.
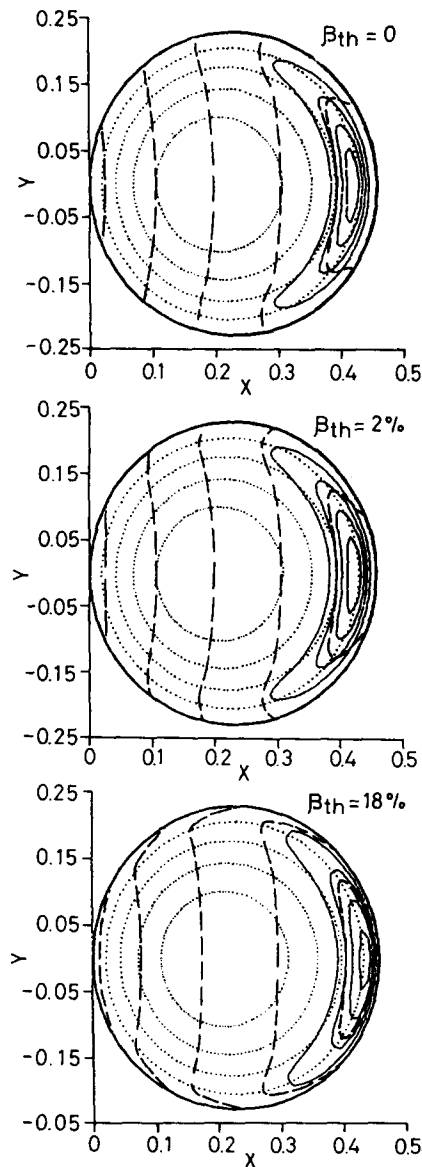

FIG. 9. The axial (Φ) magnetic flux surfaces (the nearly circular contours), the mod-B contours (the nearly vertical lines), and the hot electron pressure surfaces (the moon-shaped contours) for the reference equilibria that have $\beta_{th} = 0$ (top figure), $\beta_{th} = 2\%$ (middle figure), and $\beta_{th} = 18\%$ (bottom figure).
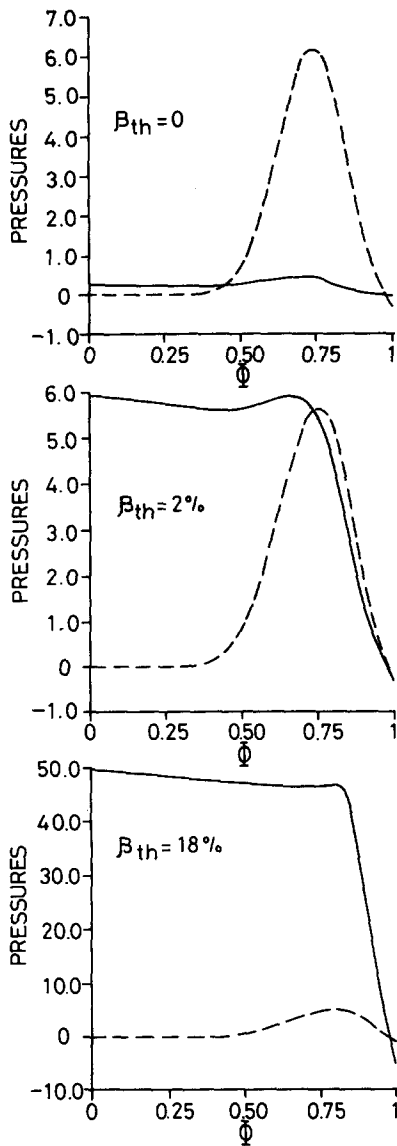
FIG. 10. The thermal pressure profiles (solid lines) and the hot electron pressure $\langle p_{\parallel} + 2p_{\perp} \rangle/3$ profiles (dashed lines) for the reference equilibria that have $\beta_{th} = 0$ (top figure), $\beta_{th} = 2\%$ (middle figure), and $\beta_{th} = 18\%$ (bottom figure) as functions of the axial magnetic flux Φ.

VII. SUMMARY AND CONCLUSIONS

In summary, we have formulated an energy functional for magnetic confinement schemes that have anisotropic plasma pressure. We have demonstrated that the variation of this energy functional with respect to an artificial time parameter reproduces the two covariant components of the MHD force balance relation that lie in planes of helical symmetry (surfaces with $\phi = $ const) in a rotating Cartesian frame. The third force component is binormal (perpendicular to the magnetic field line on a flux surface) and its vanishing makes the function (σB_{ϕ}) a constant on a flux surface. A steepest descent procedure is applied to iterate the Fourier amplitudes of the inverse coordinates $X(\rho,\theta)$ and $Y(\rho,\theta)$, and of the poloidal angle renormalization parameter $\lambda(\rho,\theta)$ to minimize the energy of the system, and as a result generate MHD equilibria with helical symmetry and anisotropic pressure.

We have implemented a computer program to construct numerical ELMO Snaky Torus MHD equilibria in the limit of helical symmetry that employs an accelerated steepest descent method. All the calculations that we have carried out have zero effective axial plasma current within each flux surface. We find that an energetic electron layer localized on the outer flux surfaces with a modest energy content $(\beta_h \simeq 0.7\%)$ can reverse the magnetic hill to a well at the outer edge of the plasma. To generate equilibria with high thermal beta (β_{th}), we tailor the thermal pressure profile so that its radial gradient is concentrated in the region where there is a magnetic well when $\beta_{th} = 0$. In the region of the magnetic hill, which is susceptible to MHD instabilities, we tailor the thermal pressure profile such that it has a weak radial gradient. This, in conjunction with the zero effective axial current condition, removes the sources of free energy that could drive these classes of modes. As a result of the small pressure gradients throughout the bulk of the plasma,
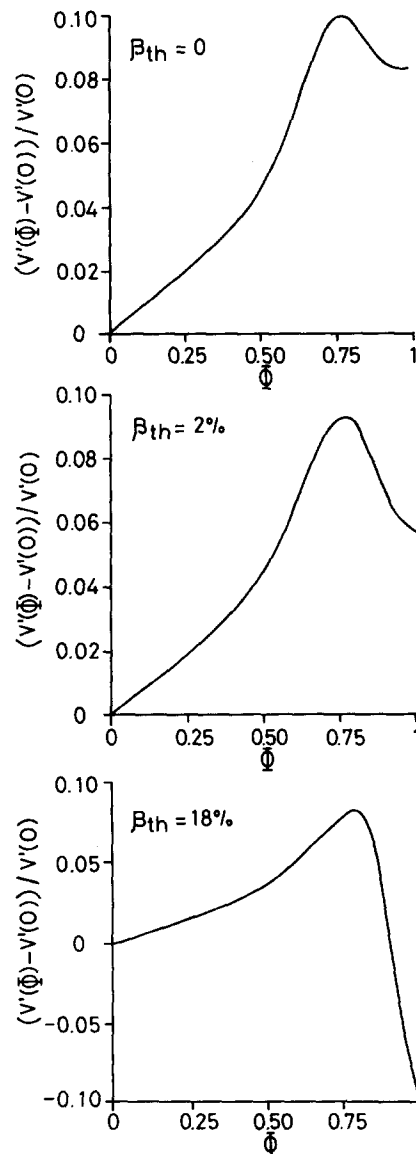

FIG. 11. The differential volume profiles for the reference equilibrium that has $\beta_{th} = 0$ (top figure), $\beta_{th} = 2\%$ (middle figure), and $\beta_{th} = 18\%$ (bottom figure) as functions of the axial magnetic flux Φ.

neither the magnetic axis nor the magnetic hill displays any perceptible change with increasing β_{th}.

ACKNOWLEDGMENTS

[1]A. Reiman and A. Boozer, Phys. Fluids **26**, 3167 (1983).
[2]D. A. Monticello, R. L. Dewar, H. P. Furth, and A. Reiman, Phys. Fluids **27**, 1248 (1984).
[3]H. P. Furth and A. Boozer, National Technical Information Service Document No. DE-84002406 (Oak Ridge National Laboratory, CONF-830758). Copies may be ordered from the National Technical Information Service, Springfield, Virginia 22161. The cost is $34.95 plus a $3.00 handling fee. All orders must be prepaid.
[4]R. A. Dandl, H. O. Eason, G. E. Guest, C. L. Hedrick, H. Ikegami, and D. B. Nelson, in *Plasma Physics and Controlled Nuclear Fusion Research* (IAEA, Vienna, 1975), Vol. II, p. 141.
[5]S. P. Hirshman and J. C. Whitson, Phys. Fluids **26**, 3553 (1983).
[6]R. L. Miller, Phys. Fluids **29**, 1176 (1986).
[7]R. L. Dewar, D. A. Monticello, and W. N.-C. Sy, Phys. Fluids **27**, 1723 (1984).
[8]M. C. Depassier and W. A. Cooper, Phys. Fluids **29**, 1948 (1986).
[9]H. Grad, in *Proceedings of Symposia in Applied Mathematics* (American Mathematical Society, Philadelphia, 1967), Vol. 18, p. 162.
[10]S. P. Hirshman and W. A. Cooper, Comput. Phys. Commun. **42**, 37 (1986).